



Strengthened caloric effect in MnCoSi under combined applications of magnetic field and hydrostatic pressure

Yao Liu¹, Zhitong Xu¹, Kaiming Qiao², Houbo Zhou², Feiran Shen², Tianzi Yang¹, Jing Wang², Tianyu Ma^{1,*} , Fengxia Hu^{2,3,*}, and Baogen Shen^{2,3}

¹ State Key Laboratory for Mechanical Behavior of Materials, and MOE Key Laboratory for Nonequilibrium Synthesis and Modulation of Condensed Matter, Frontier Institute of Science and Technology, Xi'an Jiaotong University, Xian 710049, China

² Beijing National Laboratory for Condensed Matter Physics and State Key Laboratory of Magnetism, Institute of Physics, Chinese Academy of Sciences, Beijing 100190, China

³ Songshan Lake Materials Laboratory, Dongguan 523808, Guangdong, China

Received: 18 May 2021

Accepted: 19 September 2021

Published online:

14 October 2021

© The Author(s), under exclusive licence to Springer Science+Business Media, LLC, part of Springer Nature 2021

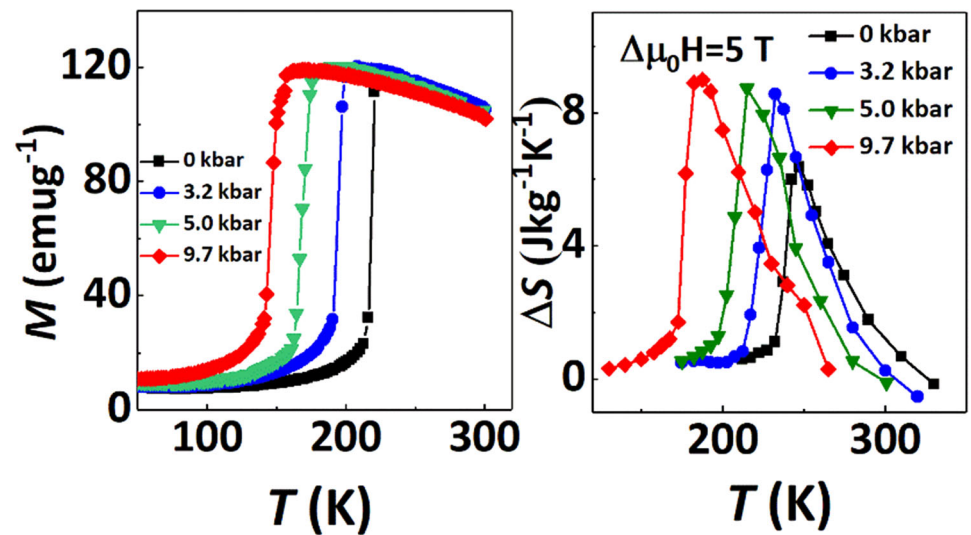
ABSTRACT

The caloric effects under combined applications of magnetic field and hydrostatic pressure to a MnCoSi meta-magnet were investigated. Under a magnetic field change of 0–5 T, the maximum magnetic entropy change was enhanced by 35.7% when a 3.2kbar hydrostatic pressure was applied, and the cooling temperature span was extended by 60 K when a hydrostatic pressure of 9.7 kbar was applied. The coupled caloric entropy change, which originates from the coupling between the magnetism and volume, was calculated and accounted for the enhanced entropy change of MnCoSi. The present work facilitates the use of MnCoSi as a solid-state refrigerant and also enriches the investigation of the multicaloric effect under multiple external fields.

Handling Editor: P. Nash.

Address correspondence to E-mail: matianyu@xjtu.edu.cn; fxhu@iphy.ac.cn

GRAPHICAL ABSTRACT



Introduction

Magnetic refrigeration based on the magnetocaloric effect (MCE) has higher theoretical energy efficiency and is more environmentally friendly than conventional vapor compression, and has attracted considerable research interest in the past few decades. Giant room temperature MCE has been reported for many materials with a magnetic field-induced first-order magneto-structural/magneto-elastic transition, such as Fe–Rh [1], $\text{Gd}_5(\text{Si,Ge})_4$ [2], $\text{La}(\text{Fe,Si})_{13}$ [3], Ni–Mn-based Heusler alloys [4], $\text{MnFeP}_x\text{As}_{1-x}$ [5, 6], and hexagonal $\text{MM}'\text{X}$ alloys (M and M' = transition metals; and X = Si, Ge, or Sn) [7]. Because of spin-lattice coupling, mechanical stress can also drive the first-order transition of these materials and result in a mechanocaloric effect (such as the barocaloric effect induced by hydrostatic pressure and the elastocaloric effect induced by uniaxial stress) [8–14]. Moreover, simultaneous or sequential application of more than one external field will give rise to the multicaloric effect [15–22]. Multicaloric effect in the aforementioned materials has attracted much interest for its priorities, such as achieving the caloric effect over a wide temperature range [18], eliminating thermal

hysteresis by transferring one control field to another and increasing the entropy change [18, 19].

MnCoSi is a meta-magnet with magneto-elastic coupling [23–27]. It has a helical antiferromagnetic (AFM) ground state and its Néel temperature is -381 K [23]. Below the Néel temperature of MnCoSi , the magnetic field can induce a meta-magnetic transition from a helical AFM to a ferromagnetic (FM) state, with simultaneous distortions of the orthorhombic lattice—where the a axis contracts and the b and c axes elongate; this transition is accompanied by a magnetostrictive effect [27] and a considerable MCE [25]. More interestingly, researchers have observed a rare Lifshitz tricritical point [28]—where paramagnetic, FM, and helicoidal AFM phases meet and the first order phase transition becomes a second-order transition in MnCoSi [23]. In materials with tricritical transition behavior, the entropic benefits of the first-order transition without a reduction of the MCE under magnetic field cycling can be used [29]. Moreover, the meta-magnetic transition of MnCoSi is sensitive to the magnetic field; the transition temperature change rate reaches -50 K T^{-1} [30]. Given the tricriticality, MnCoSi may exhibit a large reversible entropy change. Under these perspectives, MnCoSi exhibits unique priorities that may render it

useful as a magnetic refrigerant. However, corresponding studies indicate limited utility because of its low isothermal entropy change, typically $6.3 \text{ J kg}^{-1} \text{ K}^{-1}$ for a magnetic field change from 0 to 5 T [30].

Applying hydrostatic pressure (p) facilitates the meta-magnetic transition [31] and stabilizes the FM phase in MnCoSi, indicating that p can potentially act as an external field for tuning the phase transition and possibly enhancing the isothermal entropy change of MnCoSi. Hence, in our work, the multicaloric effect of MnCoSi under the combined application of a magnetic field ($\mu_0 H$) and p was studied. Under a $\mu_0 H$ change of 0–5 T, the maximum isothermal entropy change was enhanced by 35.7% when a 3.2 kbar p was loaded, compared with the isothermal entropy change measured at ambient pressure. The cooling temperature span, defined as the half-width of the maximum entropy change, was also adjusted. Our investigation on the coupled caloric effect, which accounts for the interplay between the magnetism and structure, implies that the increase in the isothermal entropy change mainly arose from the strengthened magneto-elastic coupling.

Experimental details

MnCoSi ingots were prepared by repeated arc-melting in a high-purity argon atmosphere using raw metals Mn, Co, and Si with purities greater than 99.9%. The as-prepared ingots were sealed in a vacuumed quartz tube and annealed for 60 h at 900 °C, followed by slow cooling to room temperature at a rate of $0.2 \text{ }^\circ\text{C min}^{-1}$ to release the internal strain [23]. Magnetization measurements under p were conducted with a Cu–Be high-pressure cell and Daphne 7373 as a pressure medium. The value of p was calibrated by the shift of the superconducting temperature of Pb, which was inserted concomitantly in the pressure cell with the sample. The magnetization dependence on the temperature curves (M – T) were measured in $\mu_0 H$ of 1, 3, 5, and 7 T, and isothermal magnetization curves with a temperature interval of 5 K under various values of p were measured with a Quantum Design magnetic properties measurement system. X-ray diffraction (XRD) patterns over the temperature range from 5 to 500 K were measured to identify the structural evolution upon heating.

Results and discussion

The structural evolution of MnCoSi was carefully studied by XRD at various temperatures, and the XRD patterns in Fig. 1a were refined Rietveld method using GSAS software (see S3 in supplementary materials) [32]. The results indicate that MnCoSi retained its orthorhombic structure (shown as inset Fig. 1b) over the entire measured temperature range but exhibited anisotropic lattice distortions. There was a clear change in the thermal expansion below -380 K (Fig. 1b–d); the a -axis exhibited negative thermal expansion and decreased by -0.7% , whereas the b and c axes exhibited conventional expansions. The lattice volume change with temperature is shown in Fig. 1e, it is seen that the compensation of a , b , and c axes gives rise to near-Invar-like temperature-independent behavior near 250 K, which is consistent with the previous report [1]. According to the refined structural data of MnCoSi, the two nearest-neighbor Mn–Mn distances $d1$ and $d2$ were also obtained. The $d1$ and $d2$, indicated in the inset of Fig. 1b, are critical for the magnetic state in MnCoSi, and change in opposite sense by between 1 and 2% during cooling in MnCoSi; such a drastic change in the local Mn environment serves as a precursor to the meta-magnetic transition [23, 24]. Our results are consistent with previous reports and demonstrate magneto-elastic coupling in MnCoSi [23, 24].

What's specific for MnCoSi with tricritical point is that it has a helical AFM ground state, and the Néel transition is second-order at a zero magnetic field; whereas in a high magnetic field, the second-order Néel transition becomes a first-order meta-magnetic transition from the helical AFM state to an FM state [24, 25]. The M – T curve in a small $\mu_0 H$ of 0.005 T indicates a Néel transition (Fig. 2, inset). However, the first-order meta-magnetic phase transition can be verified from the M – T curves measured in a $\mu_0 H$ of 5 T (Fig. 2). The magnetization was small in the low-temperature range and exhibited a drastic increase for heating; the reverse transition occurred for cooling with a concomitant thermal hysteresis. Moreover, MnCoSi exhibited a minor thermal hysteresis of 3 K, which implies high reversibility of the entropy change under a cycling magnetic field [29].

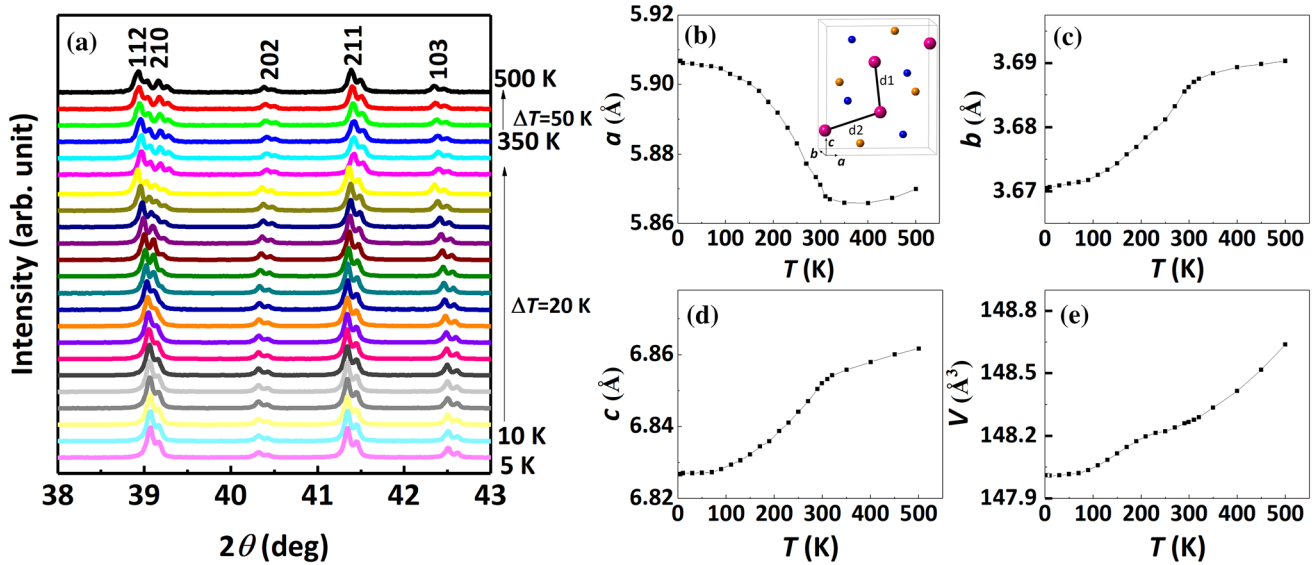


Figure 1 a XRD patterns of MnCoSi measured at various temperatures from 5 to 500 K, and b–d refined lattice parameter evolutions with temperature, e the lattice volume evolution with

temperature under no external fields, the inset in b shows the crystalline structure of MnCoSi, in which the nearest Mn–Mn bonding *d1* and *d2* are indicated.

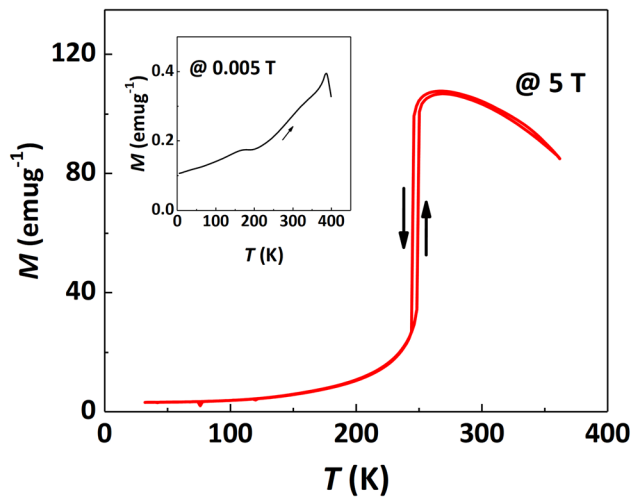


Figure 2 *M*–*T* curves with both heating and cooling plots measured in a magnetic field of 5 T; inset shows the *M*–*T* curve measured for heating at a low magnetic field of 0.005 T (upward arrow indicates heating and downward arrow indicates cooling).

Figure 3a–d shows the *M*–*T* curves measured along the heating process at ambient pressure, 3.2, 5.0, and 9.7 kbar, respectively. It is seen applying *p* stabilized the FM state in the alloy and facilitated the meta-magnetic transition at a lower μ_0H ; for example, at 9.7 kbar the meta-magnetic transition occurred even at 1 T. This fact originates from the volume contraction associated with the meta-magnetic transition from a low-temperature AFM to a high-temperature FM state [25, 30, 31]. The meta-

magnetic transition temperature (T_t) was identified as the temperature corresponding to a maximum dM/dT value in the first derivative of the *M*–*T* curves (Fig. S1 in the supplementary materials). The obtained T_t is shown as scattered spheres in Fig. 3e. By fitting the data, the combined μ_0H -dependence and *p*-dependence of T_t are as follows: $T_t(\mu_0H, p) = 396.45 - 12.43p - 47.91\mu_0H + 0.38p^2 + 3.39(\mu_0H)^2$, illustrated as the red surface in Fig. 3e. The surface separates the AFM and FM regions. Below the surface, MnCoSi is in the AFM state and above the surface, MnCoSi is in the FM state. The transition temperatures below the tricritical point were the second-order Néel transition temperatures. T_t decreased with the magnetic field, which is consistent with the literature [21]. T_t also decreased with *p*, and the rate reached -7 Kkbar^{-1} . The results indicate that both *p* and μ_0H stabilized the FM phase in MnCoSi [21].

To further investigate the effect of *p* on the MCE, the isothermal magnetization (*M*–*H*) curves of MnCoSi under various values of *p* were measured. Figures 4a and 4b show the *M*–*H* curves measured at the typical ambient pressure and 3.2 kbar, respectively. For the isotherms measured at ambient pressure, at 190 K and 200 K, the magnetization increased almost linearly under μ_0H up to 7 T, and exhibited no hysteresis between field-up and field-down plots, indicating the AFM state at these temperatures.

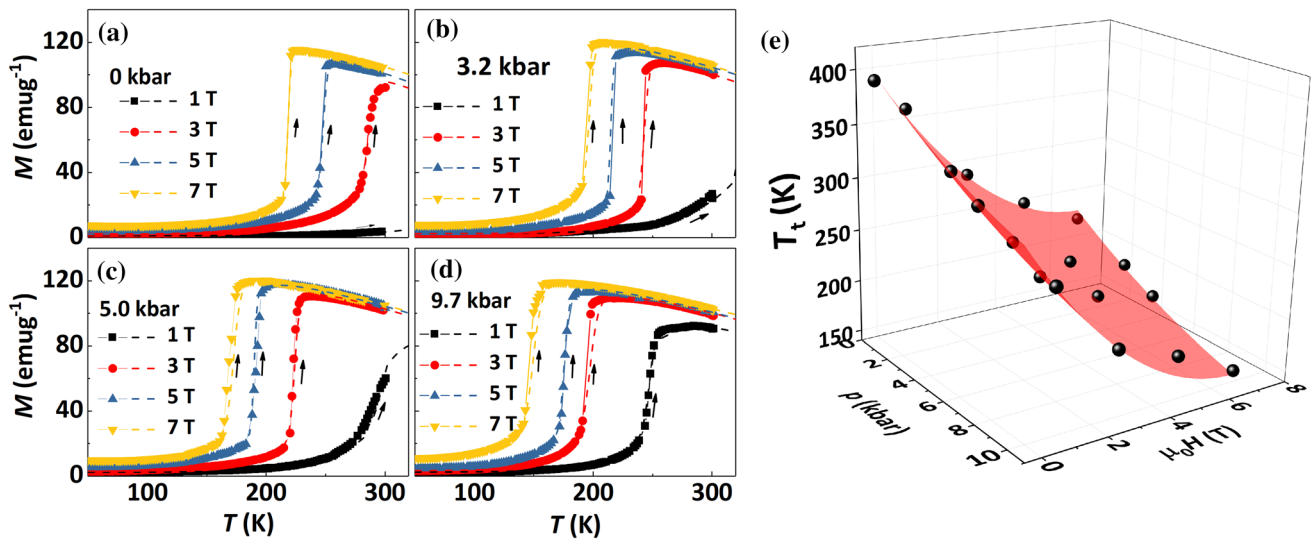
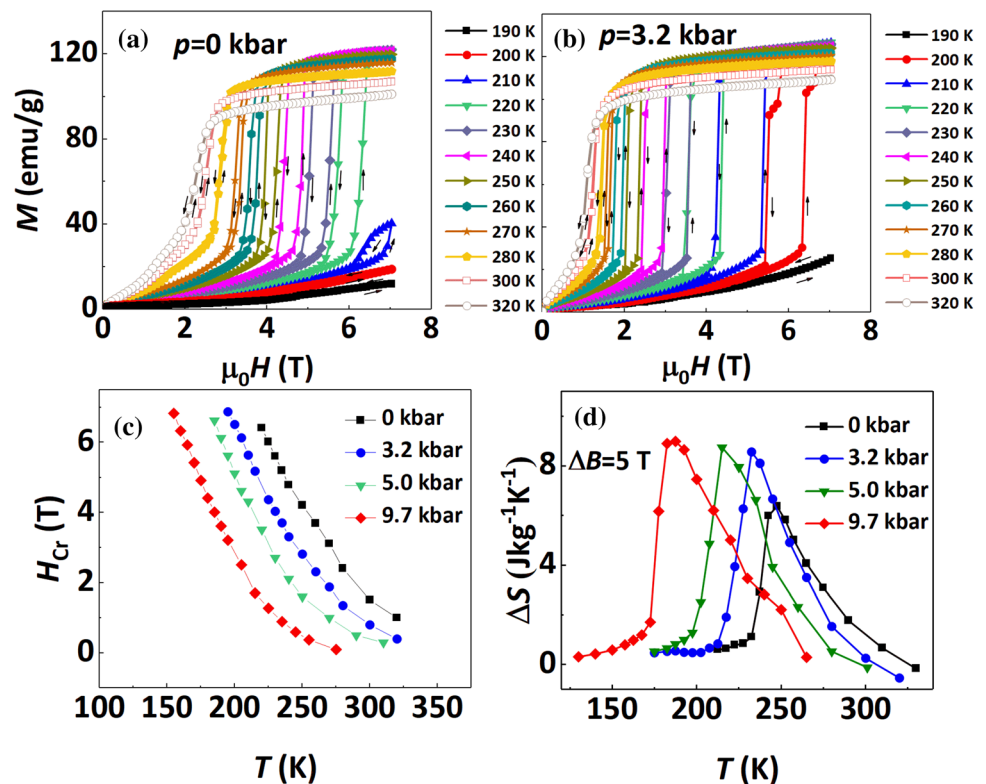


Figure 3 a–d M – T curves with heating plot measured at ambient pressure, 3.2 kbar, 5.0 kbar, and 9.7 kbar, respectively (solid lines are the experimental data whereas the dashed lines are simulated data); and e meta-magnetic transition temperature evolution under

the magnetic field and hydrostatic pressure, where the dots are the measured values and the fit red surface gives guidance regarding the separation of the AFM and FM phases.

Figure 4 a and b Isothermal M – H curves measured with a temperature interval of 10 K under ambient pressure and 3.2 kbar, respectively; c critical field for the meta-magnetic transition under fixed ambient pressure, 3.2 kbar, 5.0 kbar, and 9.7 kbar; and d magnetic entropy change for a magnetic field change of 0–5 T under fixed ambient pressure, 3.2 kbar, 5.0 kbar, and 9.7 kbar.



When heated above 210 K, the magnetization exhibited a sharp increase over a critical magnetic field (H_{Cr} , defined as a point where the magnetization is 50% of its saturation value) [26] and there was a magnetic hysteresis between the field-up and field-

down plots. These results indicate that an applied magnetic field induced a meta-magnetic transition from the AFM state to the high magnetization FM state. When further increasing the temperature to above 280 K, the magnetic hysteresis was no longer

evident, indicating that the phase transition changed to the second-order transition [23, 25]. When a 3.2 kbar p was applied, two distinct features were evident: (i) at a lower temperature of 200 K the maximum measurement μ_0H of 7 T can intrigue the meta-magnetic transition; and (ii) the H_{Cr} was reduced, as indicated by the H_{Cr} evolutions with the temperature at various values of p (Fig. 4c). The results are consistent with the observations of the M – T curves; that is, applying p stabilized the FM state in MnCoSi and thus a lowered meta-magnetic transition temperature and critical field. Based on the isotherms, the magnetic entropy changes (ΔS_M) at fixed p can be calculated through the Maxwell relation [33]:

$$\Delta S_M = \int_0^{\mu_0H} \left(\frac{\partial M}{\partial T} \right)_{p, \mu_0H} d\mu_0H. \tag{1}$$

Figure 4d shows the temperature-dependent ΔS_M curves with a fixed μ_0H change of 0–5 T at various values of p . The maximum ΔS_M was enhanced by 35.7% (i.e., from a value of $6.3 \text{ Jkg}^{-1} \text{ K}^{-1}$ at 0 kbar to a value of $8.6 \text{ Jkg}^{-1} \text{ K}^{-1}$ at 3.2 kbar) and by 42.9% (i.e., to a value of $9.0 \text{ Jkg}^{-1} \text{ K}^{-1}$ at 9.7 kbar), and the ΔS_M peak shifts to a 60 K lower temperature (i.e., from a value of 247 K to a value of 187 K) when p increased from 0 kbar to 9.7 kbar.

The aforementioned results demonstrate that both p and the magnetic field stabilized the FM phase in MnCoSi; application of a magnetic field and hydrostatic pressure in tandem enhanced the magnetic entropy change and extended the cooling temperature range of the MnCoSi alloy to a lower temperature. The multicaloric effect was studied to give an insightful understanding of the caloric effect under concomitant μ_0H and p applied to MnCoSi. Because entropy is a state function, from the thermodynamic point of view in equilibrium, there is no distinction between whether one applies the two fields simultaneously or sequentially. As a consequence, for the present case where μ_0H and p are the external stimuli, the multicaloric entropy change ΔS_{multi} is given by [18]:

$$\begin{aligned} \Delta S_{\text{multi}} &= \Delta S(T, 0 \rightarrow \mu_0H, 0 \rightarrow p) \\ &= \Delta S(T, \mu_0H = 0, 0 \rightarrow p) + \Delta S(T, 0 \rightarrow \mu_0H, p) \\ &= \Delta S_{\text{BCE}} + \Delta S(T, 0 \rightarrow \mu_0H, p). \end{aligned} \tag{2}$$

The term ΔS_{BCE} is the entropy change induced by loading p at zero magnetic field, and quantifies the standard BCE. The term $\Delta S(T, 0 \rightarrow \mu_0H, p)$ can be expressed as follows [18]:

$$\begin{aligned} \Delta S(T, 0 \rightarrow \mu_0H, p) &= \Delta S(T, 0 \rightarrow \mu_0H, 0) \\ &+ \int_0^p \frac{\partial}{\partial p'} [\Delta S(T, 0 \rightarrow \mu_0H, p')]_{T, \mu_0H} dp'. \end{aligned} \tag{3}$$

The first ΔS term to the right of the equals sign in Eq. (3) refers to ΔS_M , the entropy change induced by applying μ_0H at zero pressure, which was calculated as per Eq. (1). The second term to the right of the equals sign can further be expressed as follows [18]:

$$\begin{aligned} \Delta S_{\text{cp}} &= \int_0^p \frac{\partial}{\partial p'} [\Delta S(T, 0 \rightarrow \mu_0H, p')]_{T, \mu_0H} dp' \\ &= \int_0^p \frac{\partial}{\partial p'} \left[\int_0^{\mu_0H} \left(\frac{\partial M}{\partial T} \right)_{\mu_0H, p'} d\mu_0H \right]_{T, \mu_0H} dp' \\ &= \int_0^p \int_0^{\mu_0H} \frac{\partial}{\partial T} \left(\frac{\partial M}{\partial p} \right)_{T, \mu_0H} dp d\mu_0H, \end{aligned} \tag{4}$$

where $\chi_{12} = (\partial M / \partial p)_{T, \mu_0H}$ is the magnetic volume coupling coefficient [18]; this last term is thus the entropy change that accounts for the interplay between magnetism and volume [18]. In accordance with Eqs. (2)–(4), quantification of the caloric effect requires magnetization data over the entire (T, μ_0H, p) thermodynamic phase space.

The M – T data in Figs. 3a–d were, therefore, fit using the method reported in Ref 18. The experimental M – T curves were fit as follows. Assuming that the transition extends in temperature from $T_t - \delta T$ to $T_t + \delta T$, beyond the transition region, in the AFM region ($T < T_t - \delta T$), and in the FM region ($T > T_t + \delta T$), the temperature dependence of the magnetization can be described using an exponential function:

$$M = M_{\text{AFM}} + [M(T_t - \delta T) - M_{\text{AFM}}] \times e^{[k_1(T - T_t + \delta T)]}, T < T_t - \delta T \tag{5}$$

$$M = M_{\text{FM}} + [M(T_t + \delta T) - M_{\text{FM}}] \times [e^{[k_2(T_t - T + \delta T)]} + e^{[k_3(T - T_t)]}], T > T_t + \delta T, \tag{6}$$

where M_{AFM} and M_{FM} are the magnetization values of the AFM and FM phases, respectively; k_1 and k_2 are positive constants, while k_3 is a negative constant; and T_C is the temperature that corresponds to the inflection point where the magnetization evolution

changes from positive to negative (S4 in the supplementary materials). Within the transition region $T_i - \delta T \leq T \leq T_i + \delta T$, the M - T curves can be fit by a hyperbolic tangent function:

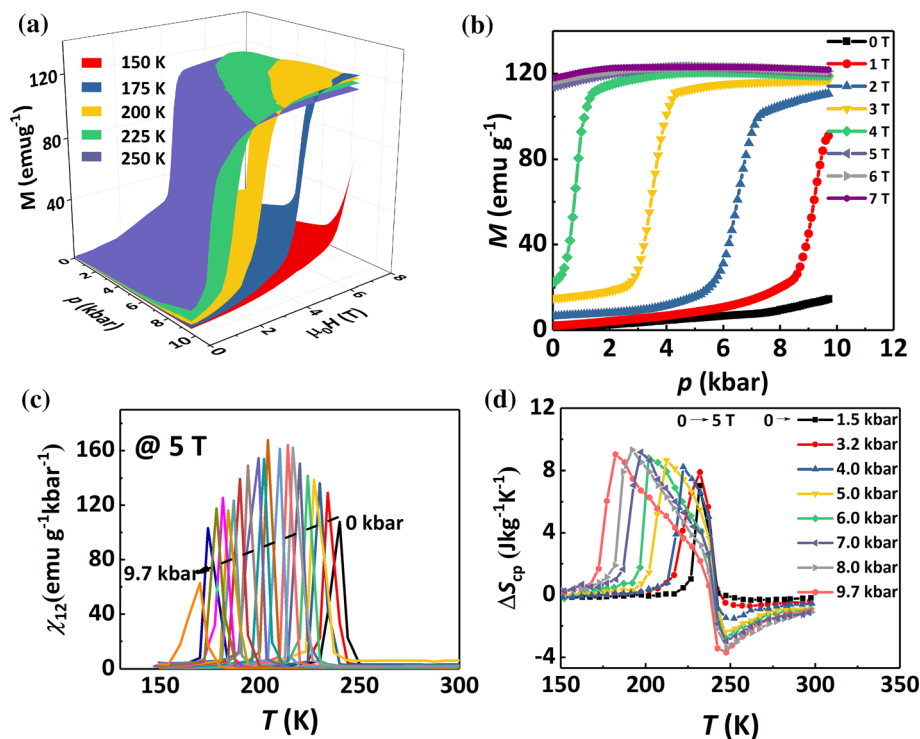
$$M = \frac{1}{2}(M_{\text{AFM}} + M_{\text{FM}}) + \frac{1}{2}(M_{\text{AFM}} - M_{\text{FM}}) \tanh\left(\frac{T - T_i}{W}\right), \quad (7)$$

where W evaluates the temperature span of the transition. The M - T curves in Figs. 3a–d were simulated and the constants and parameters in Eqs. (5)–(7) were obtained. Accordingly, M - T curves under p (0–9.7 kbar) with an interval of 0.1 kbar and $\mu_0 H$ (0–7 T) with an interval of 0.2 T were simulated. Figure 3 shows the simulation results at selected magnetic fields and hydrostatic pressures as dashed lines. The measured and simulated curves were consistent. The isothermal magnetizations with loadings of $\mu_0 H$ and p at selected temperatures were then established (Fig. S3); Fig. 5a shows the magnetization data as three-dimensional maps. To directly manifest the influence of p on the magnetization of MnCoSi, Fig. 5b shows the p dependence of the magnetization under various $\mu_0 H$ values at 250 K. It is seen that at small $\mu_0 H$ values, MnCoSi remained in the AFM state when p reached 9.7 kbar,

while at relatively high $\mu_0 H$ values from 1 T, p facilitated the meta-magnetic transition from the AFM state to the FM state. Upon further increasing the $\mu_0 H$ to 5 T, the $\mu_0 H$ has already forced the AFM state to the FM state, and the applied p reduced the magnetization slightly. The results indicate that one can use p to induce the meta-magnetic transition from the AFM state to the FM state, further confirming that p can stabilize the FM state in MnCoSi.

Based on the $M(T, p, \mu_0 H)$ data, the isothermal magnetic volume coupling coefficient χ_{12} was obtained. Figure 5c shows the χ_{12} -dependence on the temperature at 5 T and under various p values. The coupled caloric entropy change ΔS_{cp} was then calculated using the χ_{12} data as per Eq. (4). Figure 5d shows the ΔS_{cp} versus temperature curves for loadings of various p values, as well as the magnetic change from 0 to 5 T. ΔS_{cp} possesses a positive peak at low temperatures and a negative peak at high temperatures. The low-temperature positive peaks continuously increased and shifted to lower temperatures with increasing hydrostatic pressure, whereas the high-temperature negative peak remained at ~ 248 K. The absolute value increased with p and finally reached a maximum value of $6.3 \text{ Jkg}^{-1} \text{ K}^{-1}$. This negative entropy change is closely related to the evolution of χ_{12} in accordance with p and

Figure 5 **a** Isothermal magnetizations in accordance with the loading of the magnetic field and hydrostatic pressures at selected temperatures of 150 K, 175 K, 200 K, 225 K, and 250 K; **b** magnetization dependence on hydrostatic pressure at 250 K under various magnetic fields; **c** magneto-volume coefficient (χ_{12}) in accordance with the temperature in a fixed 5 T magnetic field and under various hydrostatic pressures; and **d** coupling caloric entropy change at various temperatures under magnetic field changes from 0 to 5 T, and application of various hydrostatic pressures.



T . Mathematically, at 0 kbar, χ_{12} has a maximum at T_t of 248 K and the coupled caloric effect is zero because no pressure is applied. Because of the shift of T_t to lower temperatures with increasing pressure, the maximum χ_{12} shifts to lower temperatures, and the $s\chi_{12}$ value at 248 K decreases as a result. The double integral of χ_{12} , referring to $\Delta S_{cp} = \int_0^p \int_0^{\mu_0 H} \frac{\partial}{\partial T} (\chi_{12})_{T, \mu_0 H} d\mu_0 H dp$, then results in an increasingly negative ΔS_{cp} at 248 K, which compensates for the magnetic entropy changes under 0 kbar [17]. The low-temperature positive ΔS_{cp} , on the other hand, comes from the interaction of magnetism and structure in the alloy and is responsible for the enhancement of entropy change. According to Eq. (3), the isothermal entropy change under specific pressures is the entropy change at ambient pressure adjusted by the coupled caloric entropy change. Figures 6a and b show the magnetic entropy change for a $\mu_0 H$ change of 0–5 T under fixed p values of 3.2 and 9.7 kbar; the magnetic entropy change for a $\mu_0 H$ change of 0–5 T at ambient pressure $\Delta S(T, 0 \rightarrow 5 T, 0)$; the coupled entropy change for a magnetic field change of 0–5 T and pressure change for $0 \rightarrow p$ [$\Delta S_{cp}(T, 0 \rightarrow 5 T, 0 \rightarrow p)$]; as well as the caloric entropy change calculated by $\Delta S(T, 0 \rightarrow 5 T, p) = \Delta S(T, 0 \rightarrow 5 T, 0) + \Delta S_{cp}(T, 0 \rightarrow 5 T, 0 \rightarrow p)$. The calculated $\Delta S(T, 0 \rightarrow 5 T, p)$ values for pressures of 3.2 and

9.7kbar were almost the same as the corresponding experimental isothermal magnetic entropy changes. The results thus demonstrate that the calculations of ΔS_{cp} are based on rational principles. Considering that ΔS_{cp} accounts for the interplay between the volume and magnetism degrees of freedom, the continuous increase of the low-temperature positive ΔS_{cp} peak reflects indirectly on the enforcement of the magneto-elastic coupling under increasing pressure in MnCoSi, which contributes to the enhanced entropy change when one applies p and $\mu_0 H$ [17].

The results demonstrate that extension of the cooling temperature range to lower temperatures and the enhancement of the entropy change and originate from modulation of the magneto-elastic coupling of MnCoSi by p . For the shift of meta-magnetic transition under p , usually, the applied p will stabilize the low volume phase [14, 15], which is the low temperature (low magnetization) state in MnCoSi according to Fig. 1e, however, this seems to contradict the present results that the p will lower the meta-magnetic transition temperature. This unexpected phenomenon in MnCoSi should be ascribed to the following reasons: (i) below the tricritical point (magnetic field of 2 T) [23], the transition in MnCoSi is second-order, due to which, the volume evolution with temperature under no external fields cannot be

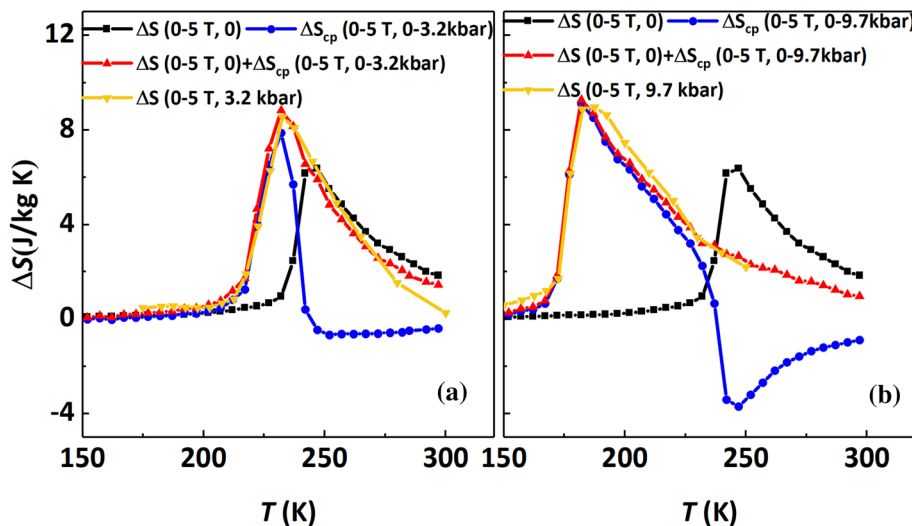


Figure 6 a and b Comparison of the entropy change for a magnetic field change of 0–5 T under a fixed pressure of 3.2 kbar and 9.7 kbar, respectively; as well as the entropy change for a magnetic field change of 0–5 T at ambient pressure adjusted by the coupled caloric entropy change. The black curve is the magnetic entropy change for a magnetic field change of 0–5 T at ambient

pressure; the blue curve is the coupled entropy change for a magnetic field change of 0–5 T, and loading of 3.2 and 9.7 kbar pressures; the red curve is the sum of the black and blue curves; and the yellow curve is the magnetic entropy change for a magnetic field change of 0–5 T under a fixed hydrostatic pressure of either 3.2 or 9.7 kbar.

used as the mere estimation of the pressure influence on the meta-magnetic transition in MnCoSi; (ii) the lattice distortion is anisotropic in MnCoSi, and the a -axis undergoing negative thermal expansion plays a dominant role in the magnetization state [23–25]. Although the structure of MnCoSi under increasing p has not been studied previously, in MnP [34] (which has a similar structure with anisotropic distortion like in MnCoSi, as well as a similar meta-magnetic transition from a helical AFM to FM phase) the compression behavior under increasing p is highly anisotropic and the decrease in the critical axis is the largest [35, 36]. Consequently, it is reasonable to infer that the critical a -axis in MnCoSi exhibits the largest compression under increasing p compared with the other axes. The decrease in the a -axis thus facilitates FM coupling in MnCoSi and reduces the meta-magnetic transition temperature of the alloy; (iii) Barcza et. al. has investigated the volume change of MnCoSi in a magnetic field by neutron diffraction, and a volume reduction of -0.3% has been obtained for the transition from the low magnetization state to high magnetization state [25], this means that when gets into first-order meta-magnetic transition, the volume evolution changes, and the low volume phase is the high magnetization state. All these facts rationalize the results that the p will stabilize the high magnetization state [31], thus reducing the meta-magnetic transition temperature and critical field. Moreover, the study on the coupled caloric entropy change demonstrates that the enhancement of entropy change stems from the enforced magneto-elastic coupling in MnCoSi. It has been revealed in MnCoSi that introducing chemical pressure (i.e., replacing Co atoms with Ni) will decrease the critical a -axis and increases the change in the a -axis during cooling, and thus causes an enforced magneto-elastic coupling [24]. Because hydrostatic pressure and chemical pressure usually have concomitant effects on the phase transition behavior in first-order, magneto-structural transition materials [37], the enforcement of magneto-elastic coupling under hydrostatic pressure could also be attributed to the decrease in the a -axis.

Conclusion

MnCoSi alloy exhibited a strengthened caloric effect under the concomitant application of a magnetic field and hydrostatic pressure. The maximum entropy changes with concomitant application of a magnetic field of 0–5 T and hydrostatic pressure of 0–9.7 kbar increased by 42.9% compared with that under application of only a 0–5 T magnetic field, and the cooling temperature range extended to a lower temperature by 60 K. Calculation of the coupled caloric entropy change, which originates from the coupling between the magnetism and volume, demonstrated that the enforced magneto-elastic coupling is responsible for the increase of the entropy change. Both the enforced magneto-elastic coupling and the modulation of the meta-magnetic transition temperature are attributable to the reduction of the critical a axis. The present work may promote the possibility of MnCoSi as a solid-state refrigerant, and also enrich the investigations of the caloric effect under multiple fields.

Acknowledgements

This work was supported by the National Natural Science Foundation of China (Nos. 51901170, 52071256, 52088101, 51971240, 51871174, U1832219, and 51771223), the open project of the Key Laboratory of Magnetic Molecules and Magnetic Information Materials of the Ministry of Education of China (No. MMMM-202003), the National Key Research and Development Program of China (Nos. 2017YFB0702702, 2019YFA0704900, and 2018YFA0305704), and the Key Program and Strategic Priority Research Program (B) of the Chinese Academy of Sciences.

Declarations

Conflict of interest The authors declare that they have no conflict of interest.

Supplementary Information: The online version contains supplementary material available at <http://doi.org/10.1007/s10853-021-06546-1>.

References

- [1] Annaorazov MP, Nikitin SA, Tyurin AL, Asatryan KA, Dovletov AK (1996) Anomalously high entropy change in FeRh alloy. *J Appl Phys* 79:1689–1695
- [2] Hu FX, Shen BG, Sun JR, Cheng ZH, Rao GH, Zhang XX (2011) Influence of negative lattice expansion and metamagnetic transition on magnetic entropy change in the compound $\text{LaFe}_{11.4}\text{Si}_{1.6}$. *Appl Phys Lett* 78:3675–3677
- [3] Pecharsky VK, Gschneidner KA Jr (1997) Giant Magnetocaloric Effect in $\text{Gd}_5\text{Si}_2\text{Ge}_2$. *Phys Rev Lett* 78:4494–4497
- [4] Krenke T, Duman E, Acet M, Wassermann EF, Moya X, Mañosa L, Planes A (2005) Inverse magnetocaloric effect in ferromagnetic Ni–Mn–Sn alloys. *Nat Mater* 4:450–454
- [5] Tegus O, Brück E, Buschow KHJ, de Boer FR (2002) Transition-metal-based magnetic refrigerants for room-temperature applications. *Nature* 415:150–152
- [6] Wada H, Tanabe Y (2001) Giant magnetocaloric effect of $\text{MnAs}_{1-x}\text{Sb}_x$. *Appl Phys Lett* 79:3302–3304
- [7] Liu EK, Wang WH, Feng L, Zhu W, Li GJ, Chen JL, Zhang HW, Wu GH, Jiang CB, Xu HB, de Boer FR (2012) Stable magnetostructural coupling with tunable magnetoresponsive effects in hexagonal ferromagnets. *Nat Commun* 3:873
- [8] Cazorla C (2019) Novel mechanocaloric materials for solid state cooling applications. *Appl Phys Rev* 6:041316
- [9] Taulats ES, Planes A, Lloveras P, Barrio M, Tamarit JL, Pramanick S, Majumdar S, Frontera C, Mañosa L (2014) Barocaloric and magnetocaloric effects in $\text{Fe}_{49}\text{Rh}_{51}$. *Phys Rev B* 89:214105
- [10] Mañosa L, González-Alonso D, Planes A, Barrio M, Tamarit JL, Titov I, Acet M, Bhattacharyya A, Majumdar S (2011) Inverse barocaloric effect in the giant magnetocaloric La–Fe–Si–Co compound. *Nat Commun* 2:595
- [11] de Medeiros LG Jr, de Oliveira NA, Troperb A (2010) Giant magnetocaloric and barocaloric effects in $\text{Mn}(\text{As}_{1-x}\text{Sb}_x)$. *J Alloy Compd* 501:177–182
- [12] Lu BF, Xiao F, Yan AR, Liu J (2014) Elastocaloric effect in a textured polycrystalline Ni–Mn–In–Co metamagnetic shape memory alloy. *Appl Phys Lett* 105:161905
- [13] Yang Z, Cong DY, Sun XM, Nie ZH, Wang YD (2017) Enhanced cyclability of elastocaloric effect in boron-microalloyed Ni–Mn–In magnetic shape memory alloys. *Acta Mater* 127:33–42
- [14] Wu RR, Bao LF, Hu FX, Wu H, Huang QZ, Wang J, Dong XL, Li GN, Sun JR, Shen FR, Zhao TY, Zheng XQ, Wang LC, Liu Y, Zuo WL, Zhao YY, Zhang M, Wang XC, Jin CQ, Rao GH, Han XF, Shen BG (2015) Giant barocaloric effect in hexagonal Ni2In-type Mn–Co–Ge–In compounds around room temperature. *Sci Rep* 5:18027
- [15] Liu J, Gottschall T, Skokov KP, Moore JD, Gutfleisch O (2012) Giant magnetocaloric effect driven by structural transitions. *Nat Mater* 11:620–626
- [16] Gong YY, Wang DH, Cao QQ, Liu EK, Liu J, Du YW (2015) Electric field control of the magnetocaloric effect. *Adv Mater* 27:801–905
- [17] Liang FX, Hao JZ, Shen FR, Zhou HB, Wang J, Hu FX, He J, Sun JR, Shen BG (2019) Experimental study on coupled caloric effect driven by dual fields in metamagnetic Heusler alloy $\text{Ni}_{50}\text{Mn}_{35}\text{In}_{15}$. *APL Mater* 7:051102
- [18] Taulats ES, Castan T, Planes A, Lewis LH, Barua R, Pramanick S, Majumdar S, Mañosa L (2017) Giant multicaloric response of bulk $\text{Fe}_{49}\text{Rh}_{51}$. *Phys Rev B* 95:104424
- [19] Gottschall T, Gràcia-Condal A, Fries M, Taube A, Pfeuffer L, Mañosa L, Planes A, Skokov KP, Gutfleisch O (2018) A multicaloric cooling cycle that exploits thermal hysteresis. *Nat Mater* 17:929–934
- [20] Meng H, Li B, Ren WJ, Zhang ZD (2013) Coupled caloric effects in multiferroics. *Phys Lett A* 377:567–571
- [21] Planes A, Taulats ES, Castán T, Vives E, Mañosa L, Saxena A (2015) Caloric and multicaloric effects in shape memory alloys. *Mater Today Proc* 2S:S477–S484
- [22] Taulats ES, Castán T, Mañosa L, Planes A, Mathur ND, Moya X (2018) Multicaloric materials and effects. *MRS Bull* 43(4):295–299
- [23] Barcza A, Gercsi Z, Knight KS, Sandeman KG (2010) Giant Magnetoelastic Coupling in a Metallic Helical Metamagnet. *Phys Rev Lett* 104:247202
- [24] Staunton JB, dos Santos Dias M, Peace J, Gercsi Z, Sandeman KG (2013) Tuning the metamagnetism of an antiferromagnetic metal. *Phys Rev B* 87:060404(R)
- [25] Barcza A, Gercsi Z, Michor H, Suzuki K, Kockelmann W, Knight KS, Sandeman KG (2013) Magnetoelastic coupling and competing entropy changes in substituted CoMnSi metamagnets. *Phys Rev B* 87:064410
- [26] Morrison K, Miyoshi Y, Moore JD, Barcza A, Sandeman KG, Caplin AD, Cohen LF (2008) Measurement of the magnetocaloric properties of $\text{CoMn}_{0.95}\text{Fe}_{0.05}\text{Si}$: large change with Fe substitution. *Phys Rev B* 78:134418
- [27] Gong YY, Liu J, Xu GZ, Xu F, Wang DH (2017) Large reversible magnetostriction in B-substituted MnCoSi alloy at room temperature. *Scr Mater* 127:165–168
- [28] Becerra CC, Shapira Y, Oliveira NF Jr, Chang TS (1980) Lifshitz point in MnP. *Phys Rev Lett* 25:1692–1695
- [29] Gutfleisch O, Gottschall T, Fries M, Benke D, Radulov I, Skokov KP, Wende H, Gruner M, Acet M, Entel P, Farle M (2016) Mastering hysteresis in magnetocaloric materials. *Philos Trans R Soc A* 374:20150308
- [30] Sandeman KG, Daou R, Özcan S, Durrell JH, Mathur ND, Fray DJ (2006) Negative magnetocaloric effect from highly

- sensitive metamagnetism in $\text{CoMnSi}_{1-x}\text{Ge}_x$. *Phys Rev B* 74:224436
- [31] Zavorotnev YD, Medvedeva LI, Todris BM, Dvornikov EA, Popova OYu (2011) Behavior of antiferromagnetic MnCoSi in a magnetic field under pressure. *J Magn Magn Mater* 323:2808–2812
- [32] Larson AC, Von Dreele RB ((2004)) General structure analysis system (GSAS), Los Alamos National Laboratory Report LAUR 86–748
- [33] Caron L, Ou ZQ, Nguyen TT, Cam Thanh DT, Tegus O, Brück E (2009) On the determination of the magnetic entropy change in materials with first-order transitions. *J Magn Magn Mater* 321:3559–3666
- [34] Reis MS, Rubinger RM, Sobolev NA, Valente MA, Yamada K, Sato K, Todate Y, Bouravleuv A, Ranke PJ, Gama S (2008) Influence of the strong magnetocrystalline anisotropy on the magnetocaloric properties of MnP. *Phys Rev B* 77:104439
- [35] Han F, Wang D, Wang YG, Li NN, Bao JK, Li B, Botana AS, Xiao YM, Chow P, Chung DY, Chen JH, Wan XG, Kanatzidis MG, Yang WG, Mao HK (2018) Spin quenching assisted by a strongly anisotropic compression behavior in MnP. *New J Phys* 20:023012
- [36] Xu YJ, Liu M, Zheng P, Chen XR, Cheng JG, Luo JL, Xie WH, Yang YF (2017) First-principles calculations of the magnetic and electronic structures of MnP under pressure. *J Phys Condens Matter* 29:244001
- [37] Caron L, Trung NT, Brück E (2011) Pressure-tuned magnetocaloric effect in $\text{Mn}_{0.93}\text{Cr}_{0.07}\text{CoGe}$. *Phy Rev B* 84:020414(R)

Publisher's Note Springer Nature remains neutral with regard to jurisdictional claims in published maps and institutional affiliations.